Simultaneous diagonal and off-diagonal order in the Bose-Hubbard Hamiltonian

R.T. Scalettar
Physics Department, University of California, Davis, California 95616

G.G. Batrouni
Groupe Matiere Condensee et Materiaux (URA 804), Universite de Rennes I, 35042 Rennes CEDEX, France

A.P. Kampf
Institut für Theoretische Physik, Universität zu Köln, 50937 Köln, Germany

G.T. Zimanyi
Physics Department, University of California, Davis, California 95616
(Received 16 September 1994)

The Bose-Hubbard model exhibits a rich phase diagram consisting both of insulating regimes where diagonal long-range (solid) order dominates as well as conducting regimes where off-diagonal long-range order (superfluidity) is present. In this paper we describe the results of quantum Monte Carlo calculations of the phase diagram, both for the hard- and soft-core cases, with a particular focus on the possibility of simultaneous superfluid and solid order. We also discuss the appearance of phase separation in the model. The simulations are compared with analytic calculations of the phase diagram and spin-wave dispersion.

I. INTRODUCTION

A lot of attention has been focused on the interacting electron problem in the last several decades, whereas the interacting boson problem has been considered more often in the framework of specific applications only. However, there are a number of important situations where the elementary excitations are either intrinsically bosonic in character or else can usefully be viewed in terms of bosonic models. ^{4}He is an example of the former situation,[1] while quantum spin systems,[2] granular superconductors,[3] and flux lines in type-II superconductors[4] are examples of the latter. Therefore it is important to understand in detail the features of model boson systems, in much the same way that one studies the Hubbard, Anderson, and t-J Hamiltonians for correlated fermions. In this paper we consider a lattice model of interacting bosons, the Bose Hubbard (BH) Hamiltonian

$$H = -t\sum_{\langle ij\rangle}(a_i^\dagger a_j + a_j^\dagger a_i) - \mu\sum_i n_i + V_0\sum_i n_i^2 + V_1\sum_{\langle ij\rangle} n_i n_j + V_2\sum_{\langle\langle ik\rangle\rangle} n_i n_k\,. \quad (1)$$

Here a_i is a boson annihilation operator at site i, and $n_i = a_i^\dagger a_i$. The transfer integral $t = 1$ sets the scale of the energy, and μ is the chemical potential. V_0, V_1, and V_2 are on-site, near-neighbor, and next-near-neighbor boson-boson repulsions.

The interactions V_0, V_1, and V_2 promote the formation of "solid" order, where the boson occupations fall into regular patterns, at special densities commensurate with the lattice. The hopping matrix element t favors mobile bosons, and consequently a superfluid phase at $T = 0$. In what follows the nature of the correlation functions will be studied as we change the Hamiltonian parameters and the density $\rho = \frac{1}{N}\sum_i\langle n_i\rangle$.

When $V_0 = \infty$, the BH model maps onto the quantum spin-1/2 Hamiltonian

$$H = -t\sum_{\langle ij\rangle}(S_i^+ S_j^- + S_j^+ S_i^-) + V_1\sum_{\langle ij\rangle} S_i^z S_j^z + V_2\sum_{\langle\langle ik\rangle\rangle} S_i^z S_k^z - H_z\sum_i S_i^z. \quad (2)$$

The field $H_z = \mu - 2V_1 - 2V_2$. Since $n_i \leftrightarrow S_i^z + \frac{1}{2}$, ordering of the density corresponds to finite wave vector Ising-type order. Similarly, $a_i \leftrightarrow S_i^-$ so that superfluidity maps to ferromagnetic ordering in the XY plane. One of the things we shall be interested in in this work is the possibility that density and superfluid order are not mutually exclusive. Indeed, at $V_2 = H_z = 0$, the special point $V_1 = 2t$ corresponds to the Heisenberg Hamiltonian where Ising and XY order coexist. It has been suggested by various authors[5,6] that the addition of further terms like V_2 or H_z could stabilize this "supersolid" from a special symmetry point to a broader area of the phase diagram. Precisely at the Heisenberg antiferromagnet (AF), the effect of a field H_z is known: It breaks the full rotational symmetry and selects ordering in the XY plane since the spins can more easily take advantage of the field energy. This argument has been used to suggest why doping favors the superconducting over the charge-

density-wave (CDW) state in the negative-U Hubbard model[7] where an analogous "supersolid" symmetry exists at half-filling.

While there have been many mean field (MF) studies of the spin Hamiltonian Eq. (2), there have been to date only a few numerical studies.[8–10] Monte Carlo studies of interacting quantum boson and spin models provide a useful, exact method to study the nature of the correlations on finite lattices. Combined with finite size scaling methods, they can be used to extract information concerning the thermodynamic limit. Boson simulations are somewhat easier than related path integral methods for interacting electron systems, since they can utilize algorithms which scale linearly with the lattice size and can reach essentially arbitrarily low temperatures.

This paper is organized as follows: In Secs. II and III we determine analytically the MF phase diagram, extending past work by considering additional types of order, and describe spin-wave calculations of the dispersion relations in the various phases. In Sec. IV we provide numerical results for the soft-core model, extending our earlier studies.[10] In Sec. V we describe results for the hard-core phase diagram. Conclusions are presented in Sec. VI.

II. MEAN FIELD PHASE DIAGRAM

Previous work established the MF phase diagram of the spin Hamiltonian considering only the possibility of superfluidity and Néel-type ordering of the density.[5,6,11] At half-filling, or equivalently at zero magnetization $M_z = 0$, for $V_1 > 2$ and $0 < V_2 < V_1 - 2$ the spins form a Néel state, corresponding to a checkerboard Bose *solid* with an ordering vector $\mathbf{k}_* = (\pi, \pi)$. For $V_2 > \max(V_1 - 2; 0)$ a ferromagnetic phase is formed, with a net moment $M_{xy} \neq 0$ and $M_z \neq 0$. This phase corresponds to a *superfluid*, and is also stable for arbitrary V_1 and V_2 away from half-filling. A fully polarized magnetic phase in a strong magnetic field H_z, where only $M_z \neq 0$, corresponds to a *Mott insulator* with precisely one boson per site. As the solid and the superfluid phases possess different broken symmetries, one could expect that the transition between them is first order. However, a rather different scenario has also been put forward, suggesting that the, presumably, first-order transition is split up into two distinct second-order transitions, where the two order parameters vanish at separate points.[11–13] In the regime between the two transitions *both* order parameters are nonzero; hence it has been termed a *supersolid*.[5,6,11] This intriguing possibility is the subject of the investigations reported in this paper.

The mean field analysis indeed finds such a supersolid phase,[5,6,11] although in the hard-core limit longer-range forces ($V_2 > 0$) are needed to stabilize it. However, recently it was claimed that this conclusion changes in the soft-core case, and a supersolid phase exists with nearest-neighbor interaction alone.[14] Finally, recent studies on the related Heisenberg model with competing first and second neighbor couplings J_1 and J_2 established the possibility of additional phases: a collinear phase, with alternating lines of up and down spins, at large J_2/J_1,[15–17] and a disordered phase at intermediate values of J_2/J_1.[18,19] These differing results clearly call for a reinvestigation of the problem.

The MF phase diagram of the spin Hamiltonian Eq. (2) worked out by Matsuda and Tsuneto,[6] and described above, allowed only for a two-sublattice magnetic ordering of the spins corresponding to a Néel solid. Representing the spins by classical vectors of length S we extend earlier MF analyses[6,20] for the case of a square lattice to include also the possibility of a collinear phase which is expected to form for intermediate to large next-nearneighbor repulsion V_2 (see Fig. 1). Assuming that the spins are ordered in the XZ plane, the MF energies per spin, e_N and e_C, of the Néel and collinear spin configurations are given by

$$e_N = -4S^2 \sin\theta_A \sin\theta_B + 2S^2 V_1 \cos\theta_A \cos\theta_B + V_2 S^2(\cos^2\theta_A + \cos^2\theta_B) - \frac{H_z}{2} S(\cos\theta_A + \cos\theta_B), \tag{3}$$

$$e_C = -S^2(\sin\theta_{R1} + \sin\theta_{R2})^2 + \frac{V_1 S^2}{2}(\cos\theta_{R1} + \cos\theta_{R2})^2 + 2V_2 S^2 \cos\theta_{R1}\cos\theta_{R2} - \frac{H_z}{2} S(\cos\theta_{R1} + \cos\theta_{R2}) . \tag{4}$$

θ_A and θ_B are the angles between the spin direction and the z axis on sublattices A and B, respectively. θ_{R1} and θ_{R2} are the corresponding angles in the collinear phase on even and odd rows. The different phases are identified as follows:

$$\begin{aligned}
\cos\theta_A = \cos\theta_B < 1 \quad \text{or} \quad \cos\theta_{R1} = \cos\theta_{R2} < 1, &\quad \text{superfluid,} \\
\cos\theta_A = -\cos\theta_B = 1, &\quad \text{Néel solid,} \\
\cos\theta_{R1} = -\cos\theta_{R2} = 1, &\quad \text{collinear solid,} \\
\sin\theta_A \neq \sin\theta_B \quad \text{and} \quad -1 < \cos\theta_A \neq -\cos\theta_B < 1, &\quad \text{Néel supersolid,} \\
\sin\theta_{R1} \neq \sin\theta_{R2} \quad \text{and} \quad -1 < \cos\theta_{R1} \neq -\cos\theta_{R2} < 1, &\quad \text{collinear supersolid,} \\
\cos\theta_A = \cos\theta_B = 1 \quad \text{or} \quad \cos\theta_{R1} = \cos\theta_{R2} = 1, &\quad \text{Mott phase.}
\end{aligned} \tag{5}$$

We performed the MF analysis in the same spirit as in Refs. 5, 6, and 11. One proceeds by minimizing e_N and e_C separately with respect to the angles θ_A, θ_B and θ_{R1}, θ_{R2}, respectively. Then the results for fixed magnetic field

H_z are translated to fixed magnetization, i.e., boson density. Finally, we compare the energies of the different phases to obtain the complete MF phase diagram of the spin Hamiltonian Eq. (2). Explicitly, for two-sublattice Néel-type ordering we find the following phases for $V_1 > 2$ and $0 < V_2 < V_1 - 2$:

$$\begin{aligned} m &= 0, \quad \text{solid}, \\ 0 < m &< \frac{1}{2}\sqrt{\frac{V_1 - V_2 - 2}{V_1 - V_2 + 2}}, \quad \text{Néel supersolid}, \\ \frac{1}{2}\sqrt{\frac{V_1 - V_2 - 2}{V_1 - V_2 + 2}} < m &< \frac{1}{2}, \quad \text{superfluid}, \\ m &= \frac{1}{2}, \quad \text{Mott insulator}, \end{aligned} \tag{6}$$

where $m = |\rho - \frac{1}{2}|$ is the magnetization of the system. For $0 < V_1 < 2$ there is no Néel order and for $m \neq 0$ the MF ground state is always superfluid.

Similarly we analyze the phase diagram following from minimizing e_C for the ordered collinear spin structures corresponding to an ordering wave vector $\mathbf{k}_* = (0, \pi)$ or $(\pi, 0)$. At half-filling the collinear solid (see Fig. 1) is realized for arbitrary values of the near-neighbor repulsion V_1. The reason is that at half-filling the energy for the collinear solid is $e_C = -V_2/2$, i.e., independent of V_1 due to the cancellation of $S_i^z S_j^z$ energies for near-neighbor sites on the same and neighboring rows. Away from half-filling only the superfluid minimizes e_C for $V_2 < 2$. For $V_2 > 2$ a collinear supersolid appears in the phase diagram and the boundary between the superfluid and the collinear supersolid is determined by

$$\begin{aligned} 0 < m &< \frac{1}{2}\sqrt{\frac{V_2 - 2}{V_2}}, \quad \text{collinear supersolid}, \\ \frac{1}{2}\sqrt{\frac{V_2 - 2}{V_2}} < m &< \frac{1}{2}, \quad \text{superfluid}, \end{aligned} \tag{7}$$

which is again independent of V_1. For $V_2 > 2$ the collinear supersolid phase occurs in a density strip of width $\sqrt{(V_2 - 2)/V_2}$ around half-filling.

Given the MF solution for e_N and e_C separately, a comparison for the energies of the different phases allows to map out the complete mean field phase diagram of the spin Hamiltonian Eq. (2). E.g., at half-filling, $m = 0$, we have to compare

$$\begin{aligned} e_C &= -\frac{1}{2}V_2, \quad \text{collinear solid}, \\ e_N &= e_C = -1, \quad \text{superfluid}, \\ e_N &= \frac{1}{2}(V_2 - V_1), \quad \text{Néel solid}. \end{aligned} \tag{8}$$

The resulting phase diagram is shown in Fig. 2. Interestingly, for $2 < V_1 < 4$ increasing V_2 drives two transitions: First increasing V_2 frustrates the Néel solid and leads to a transition to a superfluid. Increasing V_2 further stabilizes collinear order and leads to a transition from a superfluid to a collinear solid.[21]

Away from half-filling, $0 < m < 1/2$, no solids, neither Néel nor collinear, are MF solutions. Instead, transitions occur between the superfluid and the Néel and collinear *supersolid* phases. The boundaries between the different phases are given by

$$\begin{aligned} V_2 &= V_1 - 2\frac{1 + 4m^2}{1 - 4m^2}, \quad \text{superfluid to Néel supersolid}, \\ V_2 &= \frac{2}{1 - 4m^2}, \quad \text{superfluid to collinear supersolid}, \\ V_2 &= \frac{1}{2}V_1 - \frac{4m^2}{1 - 4m^2}, \quad \text{Néel to collinear supersolid}. \end{aligned} \tag{9}$$

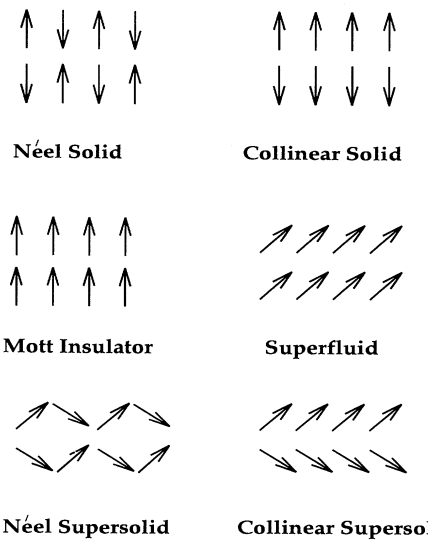

FIG. 1. Mean field phases MF of the XXZ spin Hamiltonian Eq. (2) on a 2D square lattice.

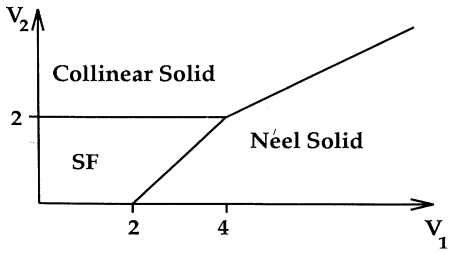

FIG. 2. Hard-core mean field phase diagram at half-filling $\rho = \frac{1}{2}$ from comparing the energies of the superfluid, and Néel and collinear solids.

Finite doping leads to a rigid shift of the phase boundary lines obtained at half-filling with the solid replaced by supersolid phases. For

$$2\frac{1+4m^2}{1-4m^2} < V_1 < 4\frac{1+2m^2}{1-4m^2}, \tag{10}$$

this still allows for two transitions with increasing V_2, from a Néel supersolid to a superfluid to a collinear supersolid. The V_1-V_2 phase diagram for a fixed magnetization $m = 0.2$ is shown in Fig. 3. In addition, Figs. 4 and 5 show the phase boundaries in the V_2, m plane for a fixed value of V_1 and in the V_1, m plane for a fixed value of V_2, respectively.

Recently it was claimed that a finite core repulsion $V_0 < \infty$ qualitatively changes this picture.[14] Supersolids were found to exist even *at half-filling*, moreover *without the next-nearest-neighbor repulsion* V_2. To study these claims we extend the MF analysis by introducing an approximate soft-core representation allowing the spin length S to be a variational parameter and adding a term $H_{\text{constraint}} = V_0 \sum_i (\mathbf{S}_i^2 - 1)^2$ to the Hamiltonian. The minimization of the ground state energy is now done separately with respect to S_x^A, S_x^B and S_z^A, S_z^B.

We expand the ground state energy around the superfluid phase, and consider the eigenvalues corresponding to small spatial modulations of the density and superfluid order parameter, in effect generating a Ginzburg-Landau-type expression. The superfluid-collinear supersolid transition is studied by writing

$$\begin{aligned} S_z^A &= m - \epsilon, & S_z^B &= m + \epsilon, \\ S_x^A &= s - \delta, & S_x^B &= s + \delta, \end{aligned} \tag{11}$$

and expanding to second order in the (small) fluctuations ϵ and δ. The expectation value e of the ground state energy per site takes the form

$$\begin{aligned} e &= e_{\text{SF}} - 4V_2\epsilon^2 + V_0[(12s^2 + 4m^2 - 1)\delta^2 \\ &\quad + (12m^2 + 4s^2 - 1)\epsilon^2 + 16sm\epsilon\delta], \\ e_{\text{SF}} &= -8s^2 + 4(V_1 + V_2)m^2 + \frac{1}{8}V_0(4s^2 + 4m^2 - 1)^2 . \end{aligned} \tag{12}$$

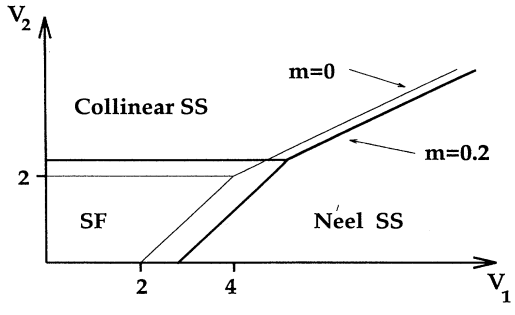

FIG. 3. Hard-core mean field phase diagram (bold lines) away from half-filling for $m = |\rho - \frac{1}{2}| = 0.2$ from comparing the energies of the superfluid and Néel and collinear supersolids. Thin lines indicate the phase boundaries at half-filling $m = 0$ (see Fig. 2).

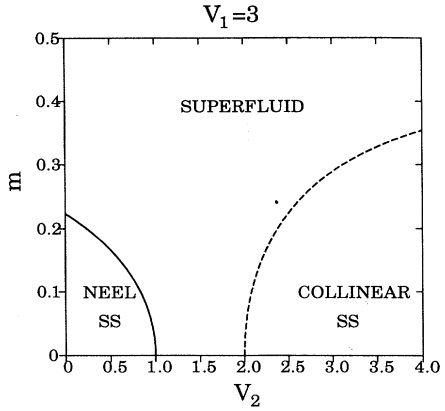

FIG. 4. Hard-core mean field phase diagram, magnetization m versus V_2, for fixed $V_1 = 3$. SS denotes the supersolid phases.

The ground state energy is the sum of eigenvalues of a matrix in the (ϵ, δ) space. First we solve for s at a fixed number of particles, i.e., fixed m, in the superconducting state where $\delta = \epsilon = 0$, and obtain

$$s^2 = \frac{1}{4} - m^2 + \frac{2}{V_0} . \tag{13}$$

A zero eigenvalue of the energy matrix signals the phase transition. The condition for the vanishing of the determinant can be solved for V_2 for arbitrary m,

$$V_2 = 2 + \frac{8m^2}{1 - 4m^2 + 12/V_0} , \tag{14}$$

which gives the phase boundary between the superfluid and the collinear supersolid. With the same procedure the phase boundary between the superfluid and the Néel supersolid is at $V_2 = V_1 - 2 - 16m^2/[1 - 4m^2 + 16/V_0]$. As in the hard-core case the phase diagram displays Néel and collinear supersolid and superfluid phases. At half-filling the supersolid phases vanish, and two insulating

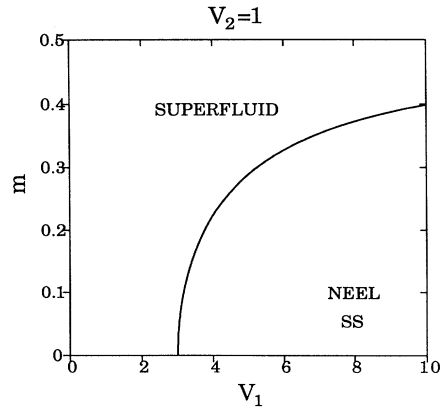

FIG. 5. Hard-core mean field phase diagram, magnetization m versus V_1, for fixed $V_2 = 1$.

solids are direct neighbors to the superfluid, in contrast with the result of Ref. 9. This result is independent of V_0; i.e., it is true both in the soft- and hard-core limits, in agreement with the above hard-core MF calculation.

III. SPIN-WAVE ANALYSIS

The analyses of the spin-wave fluctuations which exist in the literature[5,11,22] are in disagreement. The spectrum has been found to be either linear[5] or quadratic[11,22] *at* the solid-supersolid phase boundary. This dependence is crucial for numerical studies, as it determines the dynamical critical exponent z and thereby the appropriate finite size scaling of the lattice.

To settle the issue, we redo the linear spin-wave theory analysis for the spin model of Eq. (2) and determine the spectrum in the superfluid, the Néel solid, and the Néel supersolid. Again we assume that the spins are ordered in the XZ plane with an angle $\theta_{A(B)}$ to the z direction. On each sublattice the spin quantization axis is rotated to align the spins along the local direction of the magnetization by

$$\mathbf{S}_{i\in A(j\in B)} = \begin{bmatrix} \cos\theta_{A(B)} & 0 & -\sin\theta_{A(B)} \\ 0 & 1 & 0 \\ \sin\theta_{A(B)} & 0 & \cos\theta_{A(B)} \end{bmatrix} \hat{\mathbf{S}}_{i\in A(j\in B)} \,. \tag{15}$$

To diagonalize the spin Hamiltonian Eq. (2) in terms of the rotated spins $\hat{\mathbf{S}}$ we introduce spin raising and lowering operators $\hat{a}^\dagger$ and $\hat{a}$ on sublattice A by

$$\begin{aligned} \hat{S}^+_{i\in A} &= \hat{S}^x_{i\in A} + i\hat{S}^y_{i\in A} = \hat{a}^\dagger_i, \\ \hat{S}^-_{i\in A} &= \hat{S}^x_{i\in A} - i\hat{S}^y_{i\in A} = \hat{a}_i, \\ \hat{S}^z_{i\in A} &= \frac{1}{2} - \hat{a}^\dagger_i \hat{a}_i, \end{aligned} \tag{16}$$

which obey the usual bosonic commutation relations in the large S limit. Similarly, the operators $\hat{b}^\dagger$ and $\hat{b}$ are introduced on sublattice B. After Fourier transformation this leads, up to a constant energy shift, to the linear spin-wave Hamiltonian

$$\begin{aligned} H_{\rm SW} = \sum_{\mathbf{k}}{}' \Big[& H_{11}\left(\hat{a}^\dagger_{\mathbf{k}}\hat{a}_{\mathbf{k}} + \hat{a}^\dagger_{-\mathbf{k}}\hat{a}_{-\mathbf{k}}\right) + H_{33}\left(\hat{b}^\dagger_{\mathbf{k}}\hat{b}_{\mathbf{k}} + \hat{b}^\dagger_{-\mathbf{k}}\hat{b}_{-\mathbf{k}}\right) + H_{21}\left(\hat{a}^\dagger_{\mathbf{k}}\hat{a}^\dagger_{-\mathbf{k}} + \hat{a}_{\mathbf{k}}\hat{a}_{-\mathbf{k}}\right) \\ & + H_{34}\left(\hat{b}^\dagger_{\mathbf{k}}\hat{b}^\dagger_{-\mathbf{k}} + \hat{b}_{\mathbf{k}}\hat{b}_{-\mathbf{k}}\right) + H_{31}\left(\hat{a}^\dagger_{\mathbf{k}}\hat{b}_{\mathbf{k}} + \hat{a}^\dagger_{-\mathbf{k}}\hat{b}_{-\mathbf{k}} + \hat{a}_{\mathbf{k}}\hat{b}^\dagger_{\mathbf{k}} + \hat{a}_{-\mathbf{k}}\hat{b}^\dagger_{-\mathbf{k}}\right) \\ & + H_{41}\left(\hat{a}^\dagger_{\mathbf{k}}\hat{b}^\dagger_{-\mathbf{k}} + \hat{a}^\dagger_{-\mathbf{k}}\hat{b}^\dagger_{\mathbf{k}} + \hat{a}_{\mathbf{k}}\hat{b}_{-\mathbf{k}} + \hat{a}_{-\mathbf{k}}\hat{b}_{\mathbf{k}}\right)\Big], \end{aligned} \tag{17}$$

neglecting higher-order terms in $\hat{a}$ and $\hat{b}$. Due to the two-sublattice structure the $\mathbf{k}$ sum is restricted to half of the Brillouin zone, i.e., to momenta with $\cos(k_x) + \cos(k_y) \geq 0$. In the superfluid and the supersolid phases the $\mathbf{k}$-dependent coefficients in Eq. (17) are given by

$$\begin{aligned} H_{11} &= 2\frac{\sin\theta_B}{\sin\theta_A} + H_{21} \quad , \quad H_{33} = 2\frac{\sin\theta_A}{\sin\theta_B} + H_{34}, \\ H_{21} &= \frac{1}{2}V_2 \sin^2\theta_A\, \gamma^{(2)}_{\mathbf{k}} \quad , \quad H_{34} = \frac{1}{2}V_2 \sin^2\theta_B\, \gamma^{(2)}_{\mathbf{k}}, \\ H_{31} &= \gamma^{(1)}_{\mathbf{k}}\left[-1 - \cos\theta_A\cos\theta_B + \frac{1}{2}V_1 \sin\theta_A \sin\theta_B\right] \quad , \quad H_{41} = H_{31} + 2\gamma^{(1)}_{\mathbf{k}}, \end{aligned} \tag{18}$$

where $\gamma^{(1)}_{\mathbf{k}} = \frac{1}{2}[\cos(k_x) + \cos(k_y)]$ and $\gamma^{(2)}_{\mathbf{k}} = \cos(k_x)\cos(k_y)$. The coefficients of the first-order terms are required to vanish[23] which leads to the conditions

$$\begin{aligned} \frac{H_z}{2}\sin\theta_A &= 2\cos\theta_A \sin\theta_B + V_1 \cos\theta_B \sin\theta_A \\ &\quad + V_2 \cos\theta_A \sin\theta_A, \\ \frac{H_z}{2}\sin\theta_B &= 2\cos\theta_B \sin\theta_A + V_1 \cos\theta_A \sin\theta_B \\ &\quad + V_2 \cos\theta_B \sin\theta_B \,. \end{aligned} \tag{19}$$

These two equations determine the angles θ_A and θ_B for a given value of the magnetic field H_z. The solutions of Eqs. (19) determine the phase diagram of the model. These equations fully coincide with the ones obtained by minimizing the free energy in the previous section. We have already used Eq. (19) to eliminate the magnetic field in the expressions for the coefficients H_{11} and H_{33} in Eq. (18) of the spin-wave Hamiltonian. However, for the Néel solid and the Mott insulator phases where both $\sin\theta_A = 0$ and $\sin\theta_B = 0$ the elimination is not possible and instead H_{11} and H_{33} are given by

$$\begin{aligned} H_{11} &= V_1 - V_2 - \frac{1}{2}H_z, \qquad H_{33} = V_1 - V_2 + \frac{1}{2}H_z \,, \qquad \text{Néel solid}, \\ H_{11} &= H_{33} = -V_1 - V_2 + \frac{1}{2}H_z \,, \quad \text{Mott insulator}. \end{aligned} \tag{20}$$

Equation (17) is diagonalized by a generalized Bogoliubov transformation using the equation of motion $i\partial_t \hat{a}_{\mathbf{k}} = [\hat{a}_{\mathbf{k}}, H_{\mathrm{SW}}]_-$ with $\hat{a}_{\mathbf{k}} \propto e^{-i\omega_{\mathbf{k}} t}$. In the boson language the Bogoliubov transformation involves coupled density and phase modes. As a result we obtain the spin-wave dispersion in the form

$$\omega_{\pm}^2(\mathbf{k}) = \frac{1}{2}\{H_{11}^2 - H_{21}^2 + 2H_{31}^2 - 2H_{41}^2 + H_{33}^2 - H_{34}^2 \pm ((H_{11}^2 - H_{21}^2 - H_{33}^2 + H_{34}^2)^2 + 4([H_{11} - H_{21}][H_{31} + H_{41}] + [H_{33} + H_{34}][H_{31} - H_{21}]) \times ([H_{33} - H_{34}][H_{31} + H_{41}] + [H_{11} + H_{21}][H_{31} - H_{21}]))^{1/2}\}. \tag{21}$$

Typical dispersions are shown in Fig. 6 in the different phases and on the phase boundaries. We now overview the dispersion relations in the four phases.

(i) In the Néel solid which is realized for $V_2 \leq V_1 - 2$ and $H_z < 2\sqrt{(V_1 - V_2)^2 - 4}$ the spin-wave dispersion is given by

$$\omega_{\pm}(\mathbf{k}) = \sqrt{(V_1 - V_2)^2 - \left(2\gamma_{\mathbf{k}}^{(1)}\right)^2} \pm \frac{1}{2} H_z \,. \tag{22}$$

Thus, there are two excitation branches in a halved magnetic Brillouin zone. Both branches are gapped.

(ii) In the superfluid there is a Goldstone mode of linear k dependence at small k, and a well-developed minimum around $\mathbf{k}_* = (\pi, \pi)$. Taking the continuum limit carefully identifies this with the roton part of the helium dispersion. Explicitly, with $s = \sin\theta_A = \sin\theta_B$, the dispersion in the extended zone is given by

$$\omega^2(\mathbf{k}) = 2(1 - \gamma_{\mathbf{k}}^{(1)})\{2(1 - \gamma_{\mathbf{k}}^{(1)}) + s^2[V_2\gamma_{\mathbf{k}}^{(2)} + (2 + V_1)\gamma_{\mathbf{k}}^{(1)}]\}. \tag{23}$$

(iii) In the Mott insulator phase for fields $H_z > 2(2 + V_1 + V_2)$ all spins are aligned along the magnetic field direction. There is a single gapped mode in the extended first Brillouin zone with the dispersion given by

$$\omega(\mathbf{k}) = \frac{H_z}{2} - V_1 - V_2 - 2\gamma_{\mathbf{k}}^{(1)} \,. \tag{24}$$

(iv) Finally, in the supersolid phase one has a gapless linear mode, and a gapped one, again in the halved magnetic zone.

To clarify the physics of the transitions we concentrate on the dispersion at $\mathbf{k} \approx 0$ and $\mathbf{k} \approx (\pi, \pi)$ at the phase boundaries. At the supersolid-Néel-solid transition the critical mode is the Goldstone mode at small k. At the critical magnetic field $H_z^c = 2\sqrt{(V_1 - V_2)^2 - 4}$, which determines the Néel-solid–to–supersolid boundary by the vanishing of the gap of the lower excitation branch of the solid, we perform the small k expansion for $\omega_-(\mathbf{k})$ from Eq. (22). For $V_1 > V_2 + 2$ where the solid exists at half-filling we obtain

$$\omega_-(\mathbf{k}) \approx \frac{1}{2} \frac{1}{\sqrt{(V_1 - V_2)^2 - 4}} \, k^2 \,. \tag{25}$$

This means that the linear mode of the supersolid softens into a quadratic one at the boundary, signaling the destruction of superfluidity, before lifting off into a gapped mode inside the solid phase. This yields a quantum critical exponent $z = 2$. This value of z agrees with that of Chester[11] and Cheng,[22] but differs from that of Liu and Fisher,[5] who obtain $z = 1$. We feel, however, that the softening of the Goldstone mode is a physically realistic picture, supporting our result.

At the generic superfluid–to–Néel-supersolid transition the critical mode is at $\mathbf{k}_* = (\pi, \pi)$. Inside the superfluid phase the roton minimum is at this wave vector. However, in the solid, because of the zone halving, this roton minimum is folded back to $\mathbf{k} = 0$. In the superfluid where $\sin\theta_A = \sin\theta_B = s$ we study the small k expansion of the single mode in the neighborhood of $\mathbf{k} = (0, 0)$ and $\mathbf{k} = (\pi, \pi)$ (note that the Néel supersolid is only realized for $V_2 < V_1 - 2$):

$$\omega^2(\mathbf{k}) \approx \frac{s^2}{2}(2 + V_2 + V_1)\ k^2,$$
$$\omega^2[(\pi, \pi) - \mathbf{k}] \approx 8\Delta^2 + \left(2 - 3\Delta^2 - V_2 s^2\right), \tag{26}$$

where $\Delta^2 = 2 + (s^2/2)[V_2 - 2 - V_1]$. At the boundary to the Néel supersolid which is reached at a magnetic field $H_z = 2\sqrt{(V_1 - V_2)^2 - 4}(V_1 + V_2 + 2)/(V_1 - V_2 + 2)$ the mean field conditions in Eq. (19) tell that exactly at the transition the roton gap Δ disappears: *The solidification is signaled by the softening out of the roton mode of the superfluid.* The dispersion relation of the rotons also changes from a quadratic to a linear minimum; hence $z = 1$.

Two remarks are in order here. First, recalling the original Landau argument about superfluidity it is clear that a vanishing roton energy leads to a vanishing critical velocity. In other words, *upon approaching the transition from the superfluid side* the critical velocity (the slope of the line connecting the origin of the ω-k plane with the roton minimum) decreases to zero. At the same time the superfluid order parameter remains finite through the supersolid transition. *Inside* the supersolid phase the spatial periodicity is doubled, and so half of the excitation spectrum has to be folded back to the origin. This second branch acquires a gap, with a quadratic minimum above it, and so the critical velocity will continuously climb back to finite values.

Second, one can raise the question of how this picture is going to be modified in the absence of an underlying lattice. In this continuum limit the modes which go soft are located at a finite magnitude of k, i.e., on a *ring* in momentum space. This means that the phase space for these excitations is much larger than for the usual Goldstone modes, which are centered around $k \sim 0$. It then is possible that these excitations may give rise to

a fluctuation-induced first order transition instead of the second-order one taking place on the lattice.[24]

Similar expansions can be used to study the case of half-filling. In this particle-hole symmetric case, not surprisingly both transitions have $z = 1$. In a recent Monte Carlo study[9] the same z value was used in choosing the lattice size to study both the superfluid-supersolid and supersolid-solid transitions, whereas we find $z = 1$ and $z = 2$, respectively, off half-filling. Recently those simulation were repeated with these different dynamical critical exponents, and the resulting scaling curves showed considerable improvement, thereby justifying the results of

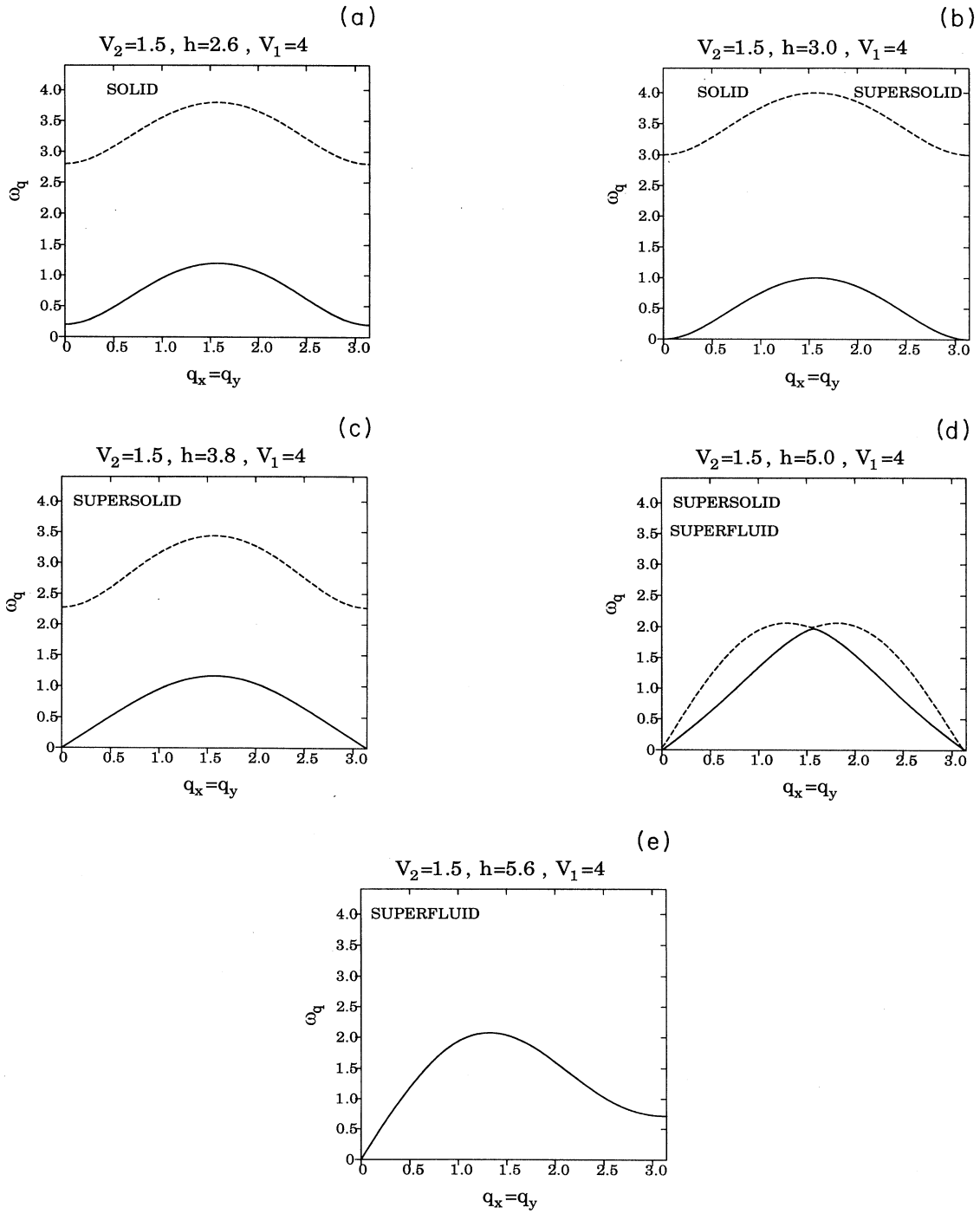

FIG. 6. Spin-wave dispersions in the (a) Néel solid, (b) at the Néel-solid–Néel-supersolid boundary, (c) in the Néel supersolid, (d) at the Néel-supersolid–superfluid boundary, and (e) in the superfluid. In all plots V_2 and V_1 are fixed to $V_2 = 1.5$, $V_1 = 4$, and the magnetic field h (H_z in the text) is varied.

the spin-wave analysis.[25]

Finally, at high fields, at the superfluid–to–Mott-insulator transition the Goldstone mode softens out again, leading to $z = 2$, in agreement with earlier field theoretical predictions[1] and numerical simulations.[26]

We have repeated the spin-wave calculation for the collinear ordering for an ordering wave vector $\mathbf{k}_* = (0, \pi)$. In this case the coefficients of the Hamiltonian Eq. (17) outside the collinear solid and the Mott insulating phases are given by

$$
\begin{aligned}
H_{11} &= \left(1 + \frac{\sin\theta_{R2}}{\sin\theta_{R1}}\right) + \frac{1}{4}\left(V_1 \sin^2\theta_{R1} - 2 - 2\cos^2\theta_{R1}\right)\cos(k_x)\,, \\
H_{33} &= \left(1 + \frac{\sin\theta_{R1}}{\sin\theta_{R2}}\right) + \frac{1}{4}\left(V_1 \sin^2\theta_{R2} - 2 - 2\cos^2\theta_{R2}\right)\cos(k_x)\,, \\
H_{21} &= \frac{1}{4}\sin^2\theta_{R1}\,(2 + V_1)\cos(k_x), \qquad H_{34} = \frac{1}{4}\sin^2\theta_{R2}\,(2 + V_1)\cos(k_x)\,, \\
H_{31} &= \frac{1}{4}\left[-2 - 2\cos\theta_{R1}\cos\theta_{R2} + V_1 \sin\theta_{R1}\sin\theta_{R2}\right]\cos(k_y) + \frac{V_2}{2}\sin\theta_{R1}\sin\theta_{R2}\,\gamma_{\mathbf{k}}^{(2)}, \\
H_{41} &= H_{31} + \cos(k_y)\,.
\end{aligned}
\tag{27}
$$

The MF conditions are read off from the vanishing of the terms linear in the spin-wave operators as before,

$$
\begin{aligned}
H_z \sin\theta_{R1} &= 2\cos\theta_{R1}(\sin\theta_{R1} + \sin\theta_{R2}) + V_1 \sin\theta_{R1}(\cos\theta_{R1} + \cos\theta_{R2}) + 2V_2 \cos\theta_{R2}\sin\theta_{R1}, \\
H_z \sin\theta_{R2} &= 2\cos\theta_{R2}(\sin\theta_{R1} + \sin\theta_{R2}) + V_1 \sin\theta_{R2}(\cos\theta_{R1} + \cos\theta_{R2}) + 2V_2 \cos\theta_{R1}\sin\theta_{R2}\,.
\end{aligned}
\tag{28}
$$

For the superfluid and the Mott insulating phase the spin-wave dispersions are obtained identical to the ones derived above in Eqs. (23) and (24). In the collinear solid with $\sin\theta_{R1} = \sin\theta_{R2} = 0$ the coefficients H_{11} and H_{33} are replaced by

$$
\begin{aligned}
H_{11} &= V_2 - \frac{1}{2}H_z - \cos(k_x), \\
H_{33} &= V_2 + \frac{1}{2}H_z - \cos(k_x)\,.
\end{aligned}
\tag{29}
$$

The two gapped modes in the collinear solid for magnetic fields $H_z \le 2\sqrt{(V_2 - 1)^2 - 1}$ and $V_2 \ge 2$ follow as

$$
\omega_{\pm}(\mathbf{k}) = \sqrt{[V_2 - \cos(k_x)]^2 - \cos^2(k_y)} \pm \frac{1}{2}H_z\,. \tag{30}
$$

As for the Néel supersolid, the collinear supersolid has one gapless linear mode at small k and a gapped one in the halved magnetic Brillouin zone which in the case of collinear ordering with wave vector $\mathbf{k}_* = (0, \pi)$ is determined by $|k_y| \le \pi/2$. The transition from the superfluid to collinear supersolid is now driven by the softening of the roton mode at $\mathbf{k}_* = (0, \pi)$. The dynamical exponent is again $z = 1$. Also the exponents at the superfluid–to–collinear-solid and at the solid-to-supersolid transition are identical to the exponents found for the Néel ordering transitions.

IV. SIMULATIONS OF THE SOFT-CORE MODEL

A. Results at half-filling

In this section we describe the results of numerical simulations, and compare them with the picture gained from the analytical considerations. Our Monte Carlo calculations are performed using a path integral representation on the BH partition function by discretizing the inverse temperature β into L_τ intervals, $\beta = L_\tau \Delta\tau$. A description of the technical details is contained in Ref. 27. In order to characterize the phase diagram, we measure the boson winding number to determine the superfluid density ρ_s. We also measure the density-density correlations $c(\mathbf{l})$ and their Fourier transform, the structure factor $S(\mathbf{k})$:

$$
\begin{aligned}
c(\mathbf{l}) &= \langle n(\mathbf{j}, \tau) n(\mathbf{j} + \mathbf{l}, \tau)\rangle, \\
S(\mathbf{k}) &= \frac{1}{N}\sum_{\mathbf{j}\,\mathbf{l}} e^{i\mathbf{k}\cdot\mathbf{l}}\,\langle c(\mathbf{l})\rangle.
\end{aligned}
\tag{31}
$$

Our normalization of the structure factor is such that if $c(\mathbf{l})$ exhibits long-range order, $S(\mathbf{k}_*)$ will be proportional to the lattice volume $N = L_x^2$, where L_x is the linear extent in the spatial dimension. If $c(\mathbf{l})$ exhibits only short-range order, $S(\mathbf{k}_*)$ will be lattice size independent. Here $\mathbf{k}_* = (\pi, \pi), (0, \pi), (\pi, 0)$ are the possible ordering wave vectors of the solid phase.

At weak coupling or high temperatures, $c(\mathbf{l})$ exhibits only short-range order. For $\mathbf{l}$ small, $c(\mathbf{l})$ is enhanced but very rapidly decays to its uncorrelated value ρ^2. However, at low temperatures for sufficiently large interactions, the density-density correlations show long-range oscillations. The associated structure factor $S(\mathbf{k})$ evolves from being rather featureless to exhibiting a sharp peak at $\mathbf{k}_* = (\pi, \pi)$ as V_1 increases, and a peak at $\mathbf{k}_* = (0, \pi)$ or $(\pi, 0)$ as V_2 increases. For our two-dimensional (2D) system, for sufficiently large V_1, we expect a transition in the Ising universality class. That is, T_c is finite. In fact, if $t = 0$, we have $T_c = 0.567\,V_1$. But even for a zero-temperature phase transition such as would occur at the Heisenberg point of the hard-core model, one will still observe "long-range order" at finite T when the di-

verging correlation length exceeds the spatial lattice size as T is lowered. In such instances, of course, a careful study of finite size effects is required to draw conclusions concerning the existence of long-range order. Here we always report results for temperatures such that $\xi > L_x$ so that observables have taken on their ground state values. We have checked the scaling behavior to be sure that the ground state is genuinely ordered, when so claimed.

Figure 7 shows the superfluid density ρ_s and structure factor $S(\pi,\pi)$ as a function of V_1 for $V_0 = 7$ and $V_2 = 0$. We see that at $V_1 \approx 2.5$ there is a phase transition from a superfluid to a solid phase. The transition on the 8×8 lattice shown is already rather sharp; finite size rounding in the raw data for the structure factor and superfluid density near the transition point is further reduced as one goes to 10×10 lattices. That one has true diagonal long-range order in the solid phase is confirmed by the fact that the structure factor scales linearly with the lattice volume. Indeed, at $V_1 = 8$, $S(\pi,\pi)$ is almost precisely 100/64 times as large on the 10×10 lattice than the 8×8. There does not appear to be any window of coexistence between the superfluid and solid phases at half-filling. To within limits set by rounding, the transition points for S and ρ_s coincide almost precisely. We can make this statement more quantitative by performing the appropriate scaling analysis on the data. For example, we have plotted $L_x^a S(\pi,\pi)$ and $L_x^b \rho_s$ versus V_1 for different values of the exponent ratios a, b. Curves for different lattice sizes should cross at the same critical value of V_1 for the appropriate choices of a, b. A complication is that the imaginary time lattice size must be scaled as the appropriate power of the spatial extent, and the dynamic exponent z could be different for the two transitions. Making the simplest assumption that z is the same, however, as was already suggested by the raw data, this scaling procedure shows that the transition points for the two observables are within 0.5% of each other. While the structure factors do indeed cross nicely, the superfluid density curves come together rather than pass through each other. This seems to be a rather generic feature of simulations of the Bose Hubbard model[28] as opposed to related conserved current models.[29,9]

As V_2 is increased, $c(\mathbf{l})$ shows a similar transition from featureless uncorrelated behavior to long-range order, although in this case V_2 favors the formation of a "striped" collinear phase with alternating lines of occupied and empty sites. The structure factor $S(\mathbf{k})$ develops a peak at $\mathbf{k}_* = (\pi, 0)$ or $(0, \pi)$.

In order to determine whether V_2 can drive a supersolid phase at half-filling, we turn on V_2 close to the point where the transition between superfluid and solid occurs in Fig. 7. The density $\rho = 0.5$. We show in Fig. 8 a plot of ρ_s and $S(\mathbf{k})$ for $\mathbf{k} = (0,\pi)$, $(\pi, 0)$, and (π,π). We see that V_2 drives the Néel solid into a superfluid, and then at yet larger values causes the formation of a striped solid phase. Again, the plots suggest that there is no supersolid phase at $\rho = 0.5$. Scaling plots similar to those constructed at $V_2 = 0$ do not reveal any evidence for distinct critical points for superfluid and solid transitions to within our numerical accuracy.

We can put data from Figs. 7 and 8 together with similar runs for different sweeps of V_1 and V_2 to obtain the ground state phase diagram of the soft-core BH model at $V_0 = 7$ and $\rho = 0.5$. This is shown in Fig. 9. At weak couplings we have a superfluid phase, while at strong couplings there are two possible solids: checkerboard and striped. A strong coupling analysis predicts a phase boundary between the solid phases at $V_2 = \frac{1}{2}V_1$. The superfluid phase extends out along this line in a very robust manner, as opposed to the situation in 1D, where the superfluid window was rather narrow.[21] This is a consequence of the highly degenerate nature of the strong coupling ($t = 0$) ground state along the line $V_1 = 2V_2$. As can easily be seen, not only do the Néel and checkerboard solids have the same energy, but an infinite number of defect states are degenerate as well for $V_1 = V_2$. For example in a horizontally aligned collinear solid a whole column can be shifted up and down without energy cost.[30,31] This large degeneracy stabilizes superfluidity, even at large coupling. We will comment further on this point when discussing the hard-core phase diagram.

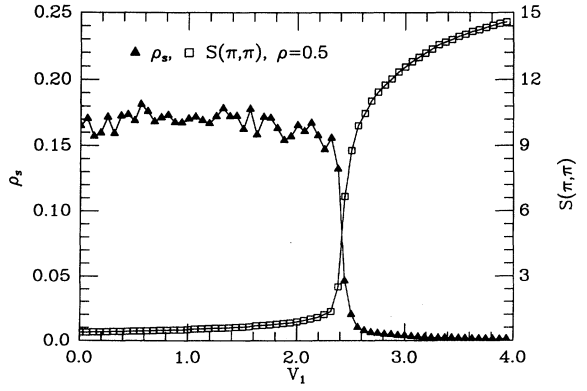

FIG. 7. The superfluid density ρ_s and $S(\pi,\pi)$ as a function of V_1 for $V_0 = 7$ and $V_2 = 0$. The density $\rho = 0.5$ and $\beta = 4$. The transitions in ρ_s and $S(\pi,\pi)$ appear to occur at roughly the same value of V_1.

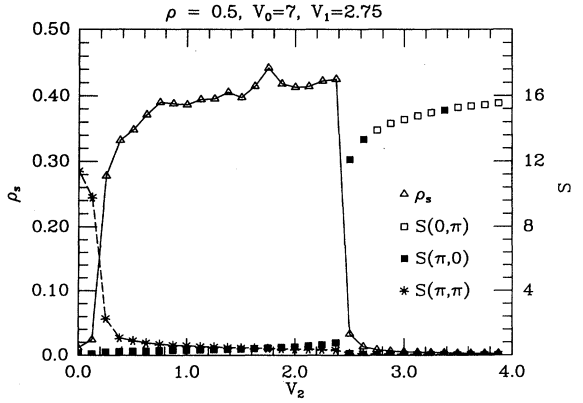

FIG. 8. The superfluid density and structure factor as a function of V_2 at $V_0 = 7$, $V_1 = 2.75$, and $\rho = 0.5$.

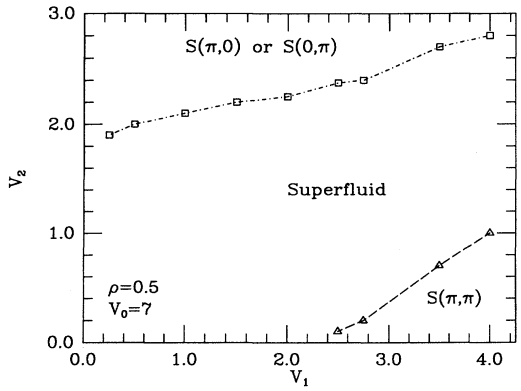

FIG. 9. The ground state phase diagram of the BH model at $\rho = 0.5$ and with a soft-core on-site repulsion $V_0 = 7$.

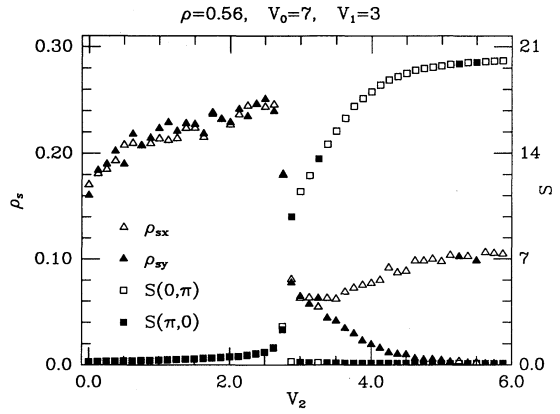

FIG. 11. The superfluid density and structure factor for the same parameters as in Fig. 8, except now the system is doped to $\rho = 0.56$. A superfluid tail remains in the (striped) solid phase.

B. Results off half-filling

Although it does not appear that the BH model exhibits a supersolid phase at $\rho = 0.5$, we can see the coexistence of diagonal and off-diagonal long-range order when the filling is shifted away from $\rho = 0.5$. In Fig. 10 we show ρ_s and $S(\pi, \pi)$ for the same parameters as Fig. 7 except now $\rho = 0.53$. We see that although ρ_s declines significantly when the solid forms, the excess boson density $\delta = \rho - 0.5$ (the magnetization m in spin language) remains mobile in the solid background. Indeed, simulations at different densities (we found supersolids out to dopings of 0.675) show that the tail in ρ_s is precisely proportional to δ. Figure 11 shows the analogous plot for a striped supersolid. Note that we have here separately displayed ρ_{sx} and ρ_{sy}. As expected, the superfluid density in the x and y directions is correlated with the direction in which the striped solid channels run, as determined by the ordering wave vector $\mathbf{k}_* = (\pi, 0)$ or $(0, \pi)$. If we had separately measured ρ_{sa} and ρ_{sb} on the two sublattices of the checkerboard solid, we would have found an analogous symmetry breaking. The nonzero value of $\rho_{sa} - \rho_{sb}$ is closely related to the appearance[5] of a nonzero order parameter $m_{xa} - m_{xb}$ in the language of the spin Hamiltonian Eq. (2).

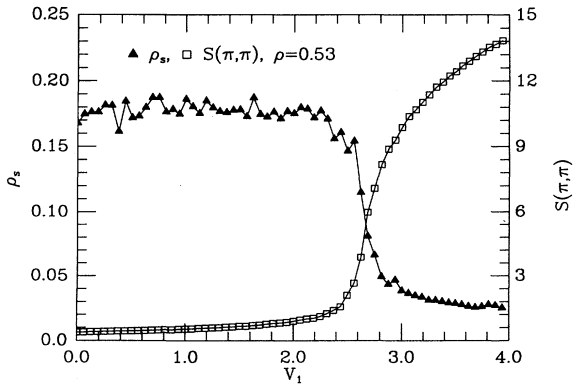

FIG. 10. The superfluid density and structure factor for the same parameters as in Fig. 7, except now the system is doped to $\rho = 0.53$. A superfluid tail remains in the (checkerboard) solid phase.

If we were to use finite size scaling techniques to locate the precise phase boundaries, it would be necessary to scale the imaginary time length L_τ as a power of the spatial length L_x^z, where z is the dynamic critical exponent. As we have earlier described, it may be that different values of z are associated with the two transitions off half-filling, in which case the finite size scaling analysis is much more delicate.[9,10] We do not see the necessity of such a study here, since the supersolid phase occupies an extended portion of the phase diagram, and its existence is not predicated on proving the distinctness of two transition points.

Figures 10 and 11 provide compelling evidence for the existence of a supersolid phase. Our physical picture of this supersolid is one in which $\rho = 0.5$ of the bosons freeze into a rigid solid structure, while the remaining δ remain mobile. As we have seen, a signal of long-range order then is present in both the diagonal $\langle n_i n_j \rangle$ and off-diagonal $\langle a_i a_j^\dagger \rangle$ channels.

We have conducted our simulations of the BH Hamiltonian in the canonical ensemble, and have presented our results by specifying the density ρ rather than the chemical potential μ. In describing the nature of the phase diagram it is important to note that due to the existence of a gap in the solid phases, the μ-ρ relation is nontrivial. If the gap is nonzero, when we dope our system even slightly away from half-filling, the chemical potential is shifted by a considerable amount. In the language of the spin Hamiltonian Eq. (2), a sizable field H_z is required to change the magnetization of the gapped Ising phase. In Fig. 12 we illustrate this point by drawing the μ/V_1-$1/V_1$ phase diagram. A sweep at constant chemical potential reveals a supersolid *window*. A sweep at fixed density skirts the pure solid and remains in the supersolid phase. This is why we see in Figs. 10 and 11 a supersolid for an extended region $V > V_{\rm crit}$ rather than in some narrow

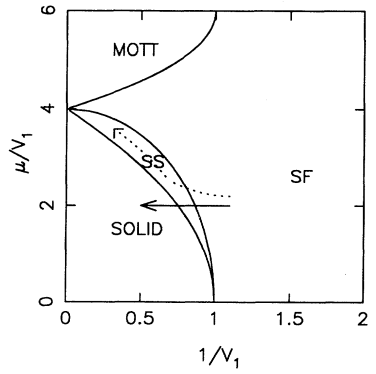

FIG. 12. The qualitative $T = 0$ phase diagram of the Bose-Hubbard model is illustrated. A sweep at constant μ (solid arrow) could cut across the phase boundaries as shown, revealing a supersolid window, while a sweep of constant density (dashed arrow) remains in the supersolid phase at strong coupling. The Mott insulating phase at large μ has a density of one boson per site.

region between phases exhibiting a single type of order.

If we now examine densities $\rho < 0.5$, we find qualitatively similar results: A superfluid phase gives way to a striped supersolid phase as V_1 increases. By these measures, hole or particle doping appears qualitatively similar. The same is true of the checkerboard supersolid, where results for hole doping are entirely reminiscent of the analogous particle doped case.

In fact, however, something rather different does go on with particle and hole doping. In Fig. 13 we show the ground state energy as a function of doping for $V_0 = 7$, $V_1 = 3$, and $V_2 = 3$. For these parameters, as we have seen, we have a striped supersolid off half-filling and a striped solid at $\rho = 1/2$. The change in slope of E_0 at $\rho = 1/2$ reflects a jump in the chemical potential which is, in fact, just the gap in the solid phase.[27] There is nothing particularly unusual here. The strange feature occurs for the checkerboard case. In Fig. 14 we show the ground state energy as a function of doping for $V_0 = 7$,

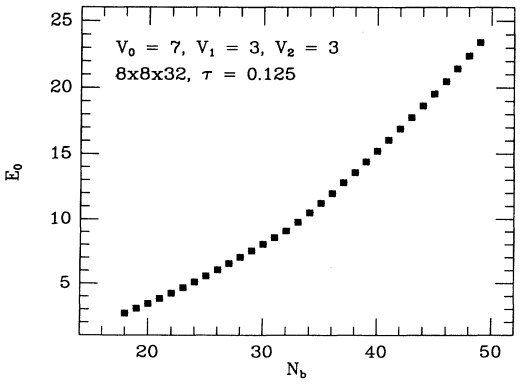

FIG. 13. The ground state energy as a function of density for $V_0 = 7$, $V_1 = 3$, $V_2 = 3$.

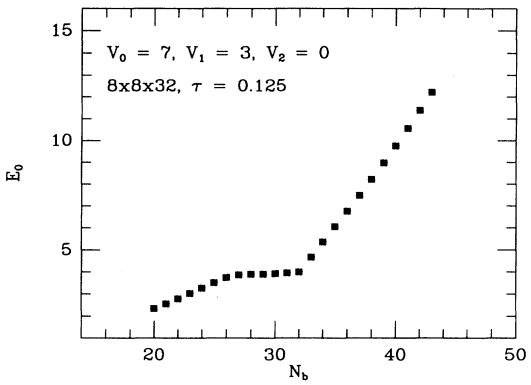

FIG. 14. The ground state energy as a function of density for $V_0 = 7$, $V_1 = 3$, $V_2 = 0$.

$V_1 = 3$, and $V_2 = 0$. The fact that $E_0(\rho)$ is concave down for $\rho < 0.5$ indicates an instability to phase separation. Previous studies[32] have suggested the possibility of phase separation in systems with attractive boson interactions. However, we do not have these Lennard-Jones-type potentials here, only purely repulsive ones. It is not immediately apparent why mobile holes (or particles) in a rigid solid background should segregate themselves.

A possible explanation, however, is as follows: Consider an isolated doped hole in a checkerboard solid. In order to move to another site of the same sublattice, it must pass through an intermediate site on the opposite sublattice, a state of energy $2V_1$. Thus the hole's effective hybridization is $t_{\text{eff}} = t^2/2V_1$. (This sort of argument has previously been used to predict the shape of the phase boundary in the one-dimensional extended BH Hamiltonian, in good agreement with simulations.[21]) If two holes are near each other, the intermediate state is lower in energy, and so the effective hybridization is increased. This suggests a possible mechanism for phase separation: increased mobility of holes which propagate coherently. Of course, the increase in t_{eff} is partially offset by the entropy cost of confining one hole near the other. Unfortunately, there appears to be an analogous increase in t_{eff} for doped particles which are proximate, and so this reasoning does not explain the fact that $E(\rho)$ is concave down for $\rho < 0.5$ only. Nevertheless, the simulations provide compelling evidence for a lack of particle-hole symmetry.

In principle, one can also examine the issue of phase separation through anomalies in $S(\mathbf{k})$ for small $\mathbf{k}$. However, our use of the canonical ensemble makes this approach nontrivial. Further work on the question of phase separation is needed.

V. SIMULATIONS OF THE HARD-CORE MODEL

We now examine the phase diagram in the hard-core case. This is important to do for a number of reasons. First, it allows us to make a connection to the spin model

limit, Eq. (2). Second, as we have seen at $V_0 = 7$, some of the interesting transitions occur at V_1 and V_2 values which are getting rather large, while we expect in most physical situations that the on-site V_0 should be substantially greater than the near-neighbor interactions. One consequence of this is that the doped bosons in the supersolid phase for our soft-core model could move on the occupied sublattice, since the cost of V_0 was less than the coordination number z times the near-neighbor interaction strengths. In the hard-core model such multiple occupancies are forbidden, and we want to make sure that our conclusions are not affected by this change.

Figure 15 shows results for the superfluid density and structure factors for the half-filled case. We sweep V_2 at fixed $V_1 = 3$. A Néel phase appears at small V_2. For larger V_2 the superfluid phase appears before making a transition into a collinear solid for yet larger V_2. If V_1 is sufficiently small, the Néel phase at weak V_2 is eliminated, and the system remains superfluid down to $V_2 = 0$. Data for this and other sweeps are summarized in Fig. 16 where the resulting ground state phase diagram is shown. Note that we find the superfluid–Néel-solid transition at $V_2 = 0$ occurs at a value V_1 close to $2t$, which is the result expected based on the mapping to the spin model, Eq. (2).

As in the soft-core case the weak coupling superfluid extends out along the $V_2 = V_1/2$ strong coupling boundary between the two solid phases. Unlike analogous studies[21] in 1D, this superfluid wedge is difficult to close, a phenomenon which we earlier explained by the large degeneracy of competing solid phases along the strong coupling line. We have conducted simulations along the line $V_2 = V_1/2$ and find that the superfluid density vanishes at $V_1 \approx 7$. Interestingly, there is no inset of solid order at this point. This needs further study, for example, to understand if some disordered dimer phase might exist in this regime, in analogy with related spin systems.

Figure 17 is a plot for a doped lattice with $\delta = \rho - 1/2 = 0.0625$. The main difference is that, as in the soft-core case, there is a superfluid tail after the structure

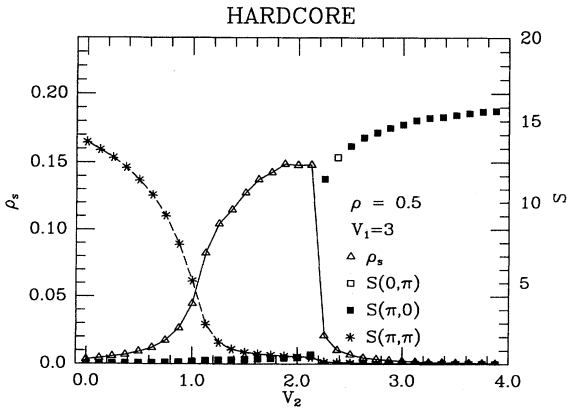

FIG. 15. Superfluid density and structure factors versus V_2 for $V_1 = 3$. The density $\rho = 0.500$.

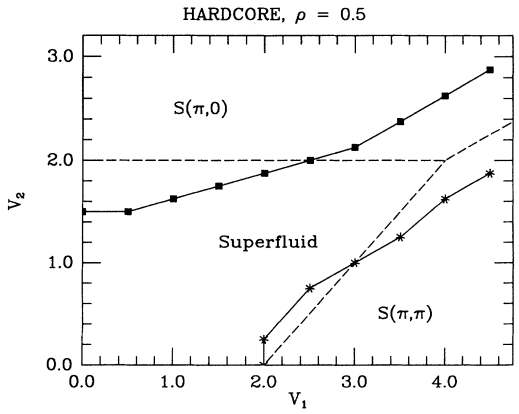

FIG. 16. The phase diagram of the half-filled hard-core model. The dashed lines are the results of the mean field analysis presented earlier in the paper.

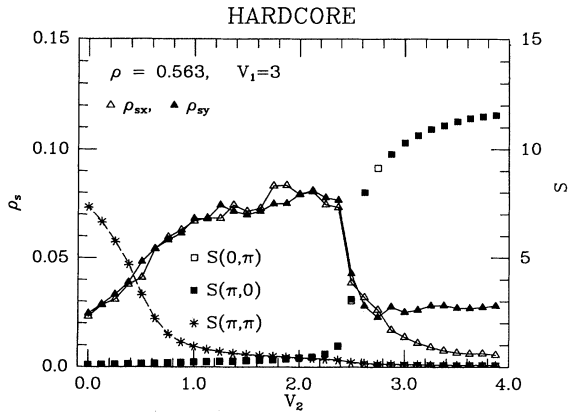

FIG. 17. Superfluid density and structure factors versus V_2 for $V_1 = 3$. The density $\rho = 0.563$.

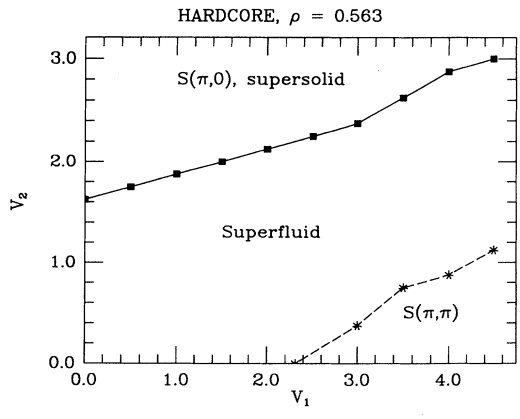

FIG. 18. The phase diagram of the doped hard-core model.

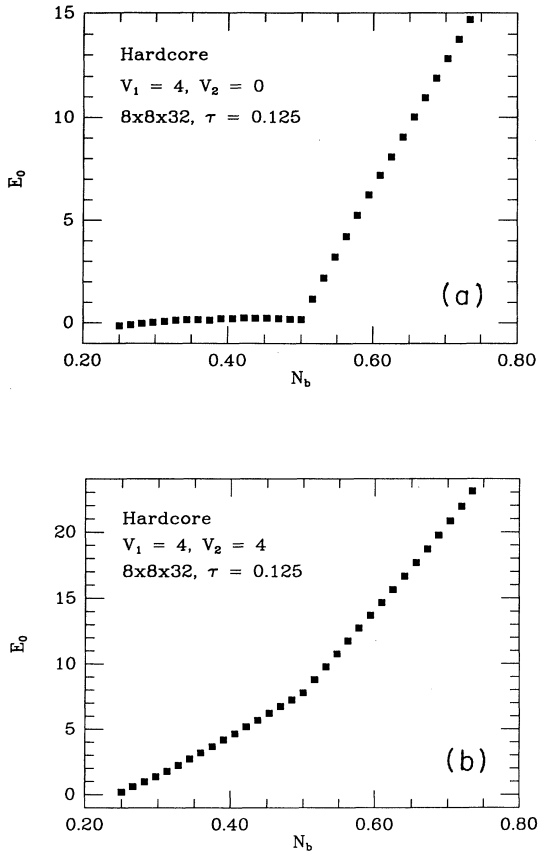

FIG. 19. Ground state energy versus density for the hard-core model. (a) $V_1 = 4, V_2 = 0$ and (b) $V_1 = 4, V_2 = 4$.

factor exhibits the transition into the solid phase. That is, there is a supersolid in the hard-core case as well. As expected, doping inhibits somewhat the formation of crystalline order, so that stronger couplings are required to induce the crystalline order as is seen by comparing the doped phase diagram, Fig. 18, with Fig. 16, the phase diagram at half-filling. Despite considerable rounding of the transitions, scaling analyses conclude that the regions where S is large are indeed ordered.

Finally, Figs. 19(a) and 19(b) show the ground state energy as a function of filling for the hard-core model at $V_1 = 8, V_2 = 0$ (Néel solid), and $V_1 = 8, V_2 = 4$ (collinear solid), respectively. The data are qualitatively similar to the soft-core model. In the collinear solid E_0 is concave up, with a change in slope at $\rho = 1/2$ which is the gap. In the Néel solid E_0 shows a tendency for phase separation.

VI. RELATED ISSUES

Up to now we have focused on the ground state phase diagram of the BH Hamiltonian. It is interesting to consider also the behavior of the system at finite temperatures. Here the motion of doped bosons in the BH model which we have studied with our simulations has a close connection with the idea of "defectons" in a solid[12] where quantum tunneling caused by the finiteness of the de Boer parameter delocalizes lattice defects at low temperature. It is also of interest to study the behavior of the diffusion constant D for the full range of temperature. Here we expect that defects are localized at high T, and D first decreases exponentially as T is lowered in this classical regime. D should then exhibit a plateau as quantum diffusion takes over, and ultimately increase again as delocalization occurs. While they focus largely on the behavior of single defectons, Andreev and Lifshitz[33] also consider the possibility of long-range Coulomb interactions causing localization into a "defecton superlattice." Our insulating checkerboard solid is in fact an illustration of this. The Bose-Hubbard model with only on-site V_0 has no solid phase at $\rho = 0.5$, but when V_1 is turned on, an ordered lattice does form.

We have focused here on zero temperature; the finite temperature phase diagram of the 2D BH model would be interesting to study as well. The solid transitions are in the Ising universality class, and hence have a finite T_c. Similarly one expects a Kosterlitz-Thouless-type finite critical temperature for the superfluid transition. As for the topology of the phase diagram, several possibilities have been explored by Liu and Fisher.[5] One intriguing case is the appearance of a tetracritical point, where the three ordered phases (superfluid, supersolid, and solid) come together, giving way to the disordered phase with further increase of the temperature. This happens within a limited, but finite range of parameters on the mean field level. The corresponding scaling theory was developed by Nelson and Fisher.[34] Other alternatives include a supersolid phase which exists only at finite temperatures, and that the tetracritical point is split into bicritical points.[5] We hope to take up some of the issues in a further publication.

In the path integral representation of the BH partition function used in our simulations, particle number conservation leads to boson "world lines" propagating in the original two spatial dimensions plus an additional imaginary time direction which runs from 0 to β. This picture has been used to suggest close analogies between the physics of vortices in type-II superconductors[35] and the phase diagram of the 2D Bose-Hubbard Hamiltonian. Frey, Nelson, and Fisher[36] have recently discussed both thermally driven and quantum phase transitions, for example, as caused by the introduction of defects or interstitials into the Abrikosov lattice, in these vortex systems. This also has close connections with the results we have discussed here.

VII. CONCLUSIONS

In this paper we have considered quantum phase transitions in the Bose-Hubbard Hamiltonian. We identified several phases: solid and supersolid phases with Néel and collinear patterns, and a superfluid and a Mott-type in-

sulating phase. The phase diagram has been determined analytically and the spin-wave spectrum has been calculated. The dynamical critical exponents at each transitions were calculated and preexisting controversies were settled. Our numerical work, utilizing quantum Monte Carlo methods, provided a detailed study of the different phases. Concerning the phase diagram the existence of supersolid phases has been forcefully confirmed. These phases exist only off half-filling, in accordance with the mean field results, but in disagreement with some recent claims. The possibility of phase separation in the model has been investigated as well, and provides evidence for a violation of the previously assumed particle-hole symmetry of the model.

ACKNOWLEDGMENTS

We acknowledge useful discussions with D. Arovas. This work was supported by the National Science Foundation Grant No. DMR 92-06023, and by Los Alamos National Laboratory under LACOR Grant No. UC-94-2-A-213. A.P.K. gratefully acknowledges support through a habilitation scholarship of the Deutsche Forschungsgemeinschaft (DFG). G.T.Z. acknowledges the kind hospitality at the University of Karlsruhe, where his work was supported by the Sonderforschungsbereich 195 of the DFG. Much of the numerical work was performed on a Connection Machine 5 at Thinking Machines Corporation.

[1] M.P.A. Fisher, P.B. Weichman, G. Grinstein, and D.S. Fisher, Phys. Rev. B **40**, 546 (1989).
[2] T. Matsubara and H. Matsuda, Prog. Theor. Phys. **16**, 569 (1956); **17**, 19 (1957).
[3] M.C. Cha, M.P.A. Fisher, S.M. Girvin, M. Wallin, and A.P. Young, Phys. Rev. B **44**, 6883 (1991).
[4] D.R. Nelson and V.M. Vinokur, Phys. Rev. Lett. **68**, 2398 (1992); Phys. Rev. B **48**, 13 060 (1993).
[5] K.S. Liu and M.E. Fisher, J. Low Temp. Phys. **10**, 655 (1973).
[6] H. Matsuda and T. Tsuneto, Suppl. Prog. Theor. Phys. **46**, 411 (1970).
[7] R.T. Scalettar, E.Y. Loh, Jr., J.E. Gubernatis, A. Moreo, S.R. White, D.J. Scalapino, R.L. Sugar, and E. Dagotto, Phys. Rev. Lett. **62**, 1407 (1989).
[8] E.Y. Loh, Ph.D. thesis, University of California, Santa Barbara, 1985.
[9] A. van Otterlo and K.-H. Wagenblast, Phys. Rev. Lett. **72**, 3598 (1994).
[10] G.G. Batrouni, R.T. Scalettar, G.T. Zimanyi, and A.P. Kampf (unpublished).
[11] G. Chester, Phys. Rev. A **2**, 256 (1970).
[12] A.F. Andreev, in *Progress in Low Temperature Physics*, edited by D.G. Brewer (North-Holland, Amsterdam, 1982), Vol. VIII.
[13] A.J. Leggett, Phys. Rev. Lett. **25**, 1543 (1970).
[14] E. Roddick and D.H. Stroud, Phys. Rev. B **48**, 16 600 (1993).
[15] R.R.P. Singh and R. Narayanan, Phys. Rev. Lett. **65**, 1072 (1990).
[16] E. Dagotto and A. Moreo, Phys. Rev. Lett. **63**, 2148 (1989).
[17] P. Chandra, P. Coleman, and A. Larkin, J. Phys. Condens. Matter **2**, 7933 (1990).
[18] N. Read and S. Sachdev, Phys. Rev. Lett. **66**, 1773 (1991).
[19] F. Figuerido *et al.*, Phys. Rev. B **41**, 4619 (1990).
[20] C. Bruder, R. Fazio, and G. Schön, Phys. Rev. B **47**, 342 (1993).
[21] P. Niyaz, R.T. Scalettar, C.Y. Fong, and G.G. Batrouni, Phys. Rev. B **44**, 7143 (1991).
[22] Y.C. Cheng, Phys. Rev. B **23**, 157 (1981).
[23] J. Kanamori and K. Yosida, Prog. Theor. Phys. **14**, 423 (1955).
[24] S. Brazovskii, Sov. Phys. JETP **41**, 85 (1975).
[25] A.V. Otterlo and K. Wagenblast (unpublished).
[26] G.G. Batrouni, R.T. Scalettar, and G.T. Zimanyi, Phys. Rev. Lett. **65**, 1765 (1990).
[27] G.G. Batrouni and R.T. Scalettar, Phys. Rev. B **46**, 9051 (1992).
[28] N. Trivedi (private communication).
[29] M. Wallin, E.S. Sorensen, S.M. Girvin, and A.P. Young, Phys. Rev. B **49**, 12 115 (1994).
[30] J. Freericks (private communication).
[31] An analysis of the related problem of possible ground states of the 2D Ising model with competing interactions is contained in U. Brandt, Z. Phys. B **53**, 283 (1983). We thank J. Freericks for bringing this reference to our attention.
[32] A. Aharony and A. Auerbach, Phys. Rev. Lett. **70**, 1874 (1993).
[33] A.F. Andreev and I.M. Lifshitz, Sov. Phys. JETP **29**, 1107 (1969).
[34] M.E. Fisher and D.R. Nelson, Phys. Rev. Lett. **32**, 1350 (1974).
[35] M.P.A. Fisher and D.H. Lee, Phys. Rev. B **39**, 2756 (1989).
[36] E. Frey, D.R. Nelson, and D.S. Fisher, Phys. Rev. B **49**, 9723 (1994).